scientific reports

Check for updates

OPEN

Utilization of indocyanine green for intraoperative sentinel lymph node mapping in canine mammary tumors

Seungwook Kim & Sungin Lee ✉

Accurate staging by sentinel lymph node (SLN) biopsy is essential for improving prognostic outcomes of canine mammary tumors (CMT). Indocyanine green near-infrared fluorescence (ICG-NIRF) imaging offers a novel real-time approach for SLN mapping, potentially enhancing the precision of surgical SLN biopsies. This study evaluated the effectiveness of transcutaneous ICG-NIRF imaging in identifying lymphatic drainage pathways and SLNs in CMT and determined the optimal ICG concentration for visualizing lymphatic channels and SLNs. We hypothesized that transcutaneous ICG-NIRF imaging effectively highlights both lymphatic channels and SLNs, facilitating accurate SLN biopsies. This study included 24 female dogs with cytologically diagnosed malignant CMT, from September 2023 to April 2024. ICG was injected peritumorally (concentrations: 0.5, 1.0, and 2.5 mg/mL). NIRF imaging was conducted intraoperatively to visualize lymphatic drainage and identify SLNs. Data on signal-to-background ratio of lymphatic drainage and SLN and operation time were collected and analyzed using ANOVA and post-hoc Tukey tests. The detection rate of SLNs using ICG-NIRF was 94.4% (34/36). Highest LN fluorescence ($p = 0.030$) and shortest operation time ($p = 0.002$) were yielded by 1.0 mg/mL ICG, with minimal false-negative rates (0%, 0/18). ICG-NIRF imaging enhances the accuracy of sentinel lymph node mapping in CMT by enabling real-time visualization of lymphatic drainage, optimizing lymph node biopsy selection, and improving surgical precision, thereby contributing to more accurate tumor staging and better prognostic assessment.

Keywords Canine, ICG-NIRF, Lymphatic drainage, Mammary tumors, Optimal ICG concentration, SLN mapping

Canine mammary tumors (CMT) represent a significant proportion of all canine neoplasms, accounting for approximately 47 to 60% of the tumors in female dogs[1–3]. Diagnosis is made using fine-needle aspiration (FNA) and clinical staging using the tumor-node-metastasis (TNM) classification system for malignancies is important in prognostic assessment[4,5]. Clinical staging includes three-view thoracic radiographs and FNA of the regional lymph nodes (LNs). Surgical resection is recommended for CMT, except for inflammatory mammary carcinoma or presence of distant metastases, and histopathology confirms the types of CMT[4].

A sentinel lymph node (SLN) refers to the initial LN in the lymphatic drainage that receives drainage from the primary tumor. SLN mapping is a precise technique for identifying LNs potentially affected by metastatic spread[6]. Precise staging can be challenging, because lymphatic drainage patterns are not always consistent with anatomical locations[6]. Identifying SLN allows less invasive surgical dissection, more accurate LN extirpation, and improved overall outcomes[7]. Histological analysis of tissue samples provides the most precise staging information for canine patients, guiding treatment decisions and prognostication. In human cancer surgery, SLN biopsy is a standardized procedure, whereas, in veterinary practice, LN removal is often performed when the nodes are enlarged or confirmed as tumor-positive by FNA. However, clinically observed LN enlargement does not always correlate with pathophysiological metastasis[8]. Normal canine LNs are only a few millimeters in size, making them difficult to detect visually. Various imaging techniques, including indirect computed tomographic lymphography (ICTL)[9], patent blue dye[10], lymphoscintigraphy[11]and contrast-enhanced ultrasound[12], have been employed to visualize these nodes.

Department of Veterinary Surgery, College of Veterinary Medicine, Chungbuk National University, Cheongju 28644, Korea. ✉email: sunginlee@cbnu.ac.kr

Near-infrared fluorescence (NIRF) imaging is an emerging clinical technology that relies on the administration of a fluorescent imaging agent capable of excitation at near-infrared wavelengths greater than 760 nm. Indocyanine green (ICG), an FDA-approved fluorescent contrast agent, has an emission peak at 822 nm[13]. ICG-NIRF imaging has been successfully applied in humans for SLN mapping in various cancers including melanoma and, breast, cervical, gastric, skin, and vulvar cancers[13]. Its use in veterinary sentinel lymph node mapping is also being actively investigated, showing potential for broader application[12,14–16]. This imaging modality holds promise for enhancing SLN mapping by facilitating the real-time transcutaneous visualization of lymphatic channels, thereby aiding the detection of SLNs during surgical procedures.

The objective of this study was to demonstrate the application of NIRF imaging with transcutaneous injection of ICG to identify the lymphatic drainage pathways and SLNs associated with CMT. Additionally, this study aimed to determine the optimal ICG concentration for visualizing the lymphatic channels and SLNs in CMT while minimizing operation time. We hypothesized that ICG-NIRF would effectively highlight the lymphatic channels and SLNs, facilitating SLN biopsies. Furthermore, we aimed to identify the optimal ICG concentration by evaluating its effectiveness in SLN mapping and its impact on operation time.

Results

Study population

A total of 36 LNs (26 inguinal and 10 axillary) and 38 CMTs from 24 female dogs were included in this study. The clinical data of the canine patients including breed, age, sex, body weight, and BCS are listed in Table 1.

The breeds of the included dogs were Maltese ($n=7$), Poodle ($n=5$), Pomeranian ($n=3$), Mixed breed ($n=3$), Beagle ($n=1$), Bichon Frise ($n=1$), Boston Terrier ($n=1$), Doberman Pinscher ($n=1$), Pekingese ($n=1$), and Pungsan ($n=1$). Nine dogs were intact, and 15 were neutered. The mean age was 11.3 years, with a median age of 11.7 years (95% CI, 10.1–12.4). The mean body weight was 6.8 kg, with a median body weight of 4.0 kg (95% CI, 3.8–9.8). The median BCS was 5 (range, 4–7). There were no statistically significant differences in age ($p=0.298$), body weight ($p=0.327$), BCS ($p=0.293$), or tumor size ($p=0.437$) between the groups with different ICG concentrations.

Tumor characteristics

Histopathological examinations of the resected tumors and LNs were conducted. Table 2 shows the distribution of tumor location, size, draining LN, histopathology, grade, and presence of LN metastasis.

The mean and median tumor diameters were 26.3 mm and 12.0 mm, respectively (95% CI, 15.6–36.9). The tumor locations included the right fourth mammary gland (MG; $n=9$), right third MG ($n=7$), right fifth MG ($n=5$), left third MG ($n=4$), left fourth MG ($n=4$), left fifth MG ($n=4$), left second MG ($n=3$), right first MG ($n=1$), and right second MG ($n=1$). Efferent lymphatic drainage was performed on the ipsilateral axillary LNs ($n=4$) for the first and second MG, and ipsilateral ($n=17$) and contralateral ($n=4$) inguinal LNs for the fourth and fifth MG. The lymphatic channel of the third MG drained into the either ipsilateral axillary LNs ($n=6$) or ipsilateral inguinal LNs ($n=5$). The tumor types included solid carcinoma ($n=10$), benign mixed tumor ($n=9$), complex adenoma ($n=6$), complex carcinoma ($n=5$), carcinosarcoma ($n=2$), anaplastic carcinoma ($n=1$), fibroadenoma ($n=1$), osteosarcoma ($n=1$), simple adenoma ($n=1$), spindle cell carcinoma ($n=1$), and tubulopapillary carcinoma ($n=1$). Most malignant tumors were classified as grade I (57.1%, 12/21), followed by grade III (38.1%, 8/21), and grade II (4.8%, 1/21). LN metastases were observed in 11.1% (4/36) of nodes considered SLNs.

ICG-NIRF SLN biopsy with different ICG concentrations

Fluorescence in the lymphatic channels became visible within 5 min post-injection. The exact duration of fluorescence retention could not be determined, as sentinel lymph node resection was completed within 30 min in all cases. However, fluorescence remained visible for at least 30 min without a notable decrease in intensity.

Case No.	Breed	Age (year)	Gender	Weight (kg)	BCS	Case No.	Breed	Age (year)	Gender	Weight (kg)	BCS
1	Pungsan	13.0	IF	28.5	7	13	Beagle	4.8	IF	13.4	5
2	Poodle	13.2	IF	7.0	6	14	Maltese	9.4	SF	3.6	5
3	Maltese	11.4	SF	2.5	5	15	Mixed	5.9	IF	9.0	5
4	Boston Terrier	7.0	IF	8.3	6	16	Doberman Pinscher	10.0	IF	28.3	4
5	Pomeranian	13.2	SF	1.5	4	17	Mixed	9.0	IF	4.8	5
6	Pekingese	15.4	SF	7.0	5	18	Maltese	9.6	SF	3.2	5
7	Pomeranian	10.0	SF	4.0	7	19	Poodle	13.0	SF	4.6	5
8	Poodle	10.0	SF	5.4	5	20	Maltese	12.0	SF	3.0	7
9	Bichon Frise	13.0	SF	6.6	7	21	Mixed	14.8	SF	2.8	5
10	Maltese	13.7	SF	2.8	5	22	Maltese	10.8	IF	4.0	6
11	Poodle	13.0	IF	3.8	4	23	Maltese	11.0	SF	3.5	6
12	Poodle	13.6	SF	3.8	6	24	Pomeranian	14.0	SF	2.5	6

Table 1. Signalment of canine mammary tumor canine patients included in this study. BCS, body condition score; LN, lymph node; IF, intact female; SF, spayed female; Lt, left; Rt, right; N/A, not available

Case No.	Tumor Location	Tumor size in diameter (mm)	ICG concentration (mg/mL)	Draining LN	Tumor Histopathology	Grade	LN metastasis
1	Lt. M3 Lt. M5 Rt. M3	82 87 36	2.5	Lt. inguinal ln Lt. inguinal ln Rt. inguinal ln	Solid carcinoma Solid carcinoma Complex carcinoma	III III III	Present Absent
2	Lt. M2	32	2.5	Lt. axillary ln	Solid carcinoma	I	Absent
3	Lt. M5 Rt. M5	10 11	2.5	Lt. inguinal ln Rt. inguinal ln	Complex carcinoma Complex carcinoma	I I	Absent Absent
4	Rt. M4	5	2.5	Lt. inguinal ln	Benign mixed tumor		Absent
5	Lt. M5	7	2.5	Lt. inguinal ln	Complex adenoma		Absent
6	Rt. M5	37	2.5	Rt. inguinal ln	Solid carcinoma	II	Absent
7	Rt. M4	11	2.5	Lt. inguinal ln	Tubulopapillary carcinoma	I	Absent
8	Lt. M4 Rt. M3	6 6	1.0	Lt. inguinal ln Rt. inguinal ln	Benign mixed tumor Benign mixed tumor		Absent Absent
9	Rt. M5	65	1.0	Lt. inguinal ln	Solid carcinoma	I	Absent
10	Rt. M3	11	1.0	Rt. axillary ln	Solid carcinoma	I	Absent
11	Lt. M2 Rt. M3 Rt. M4	6 13 28	1.0	Lt. axillary ln Rt. axillary ln Rt. inguinal ln	Complex adenoma Complex adenoma Benign mixed tumor		Absent Absent Absent
12	Lt. M4	5	1.0	Rt. inguinal ln	Solid carcinoma	I	Absent
13	Lt. M2 Rt. M3 Rt. M4	55 37 11	1.0	Lt. axillary ln Rt. axillary ln Rt. inguinal ln	Solid carcinoma Solid carcinoma Solid carcinoma	I I I	Absent Absent Absent
14	Rt. M2 Rt. M4	5 16	1.0	Rt. axillary ln Rt. inguinal ln	Simple adenoma Osteosarcoma	III	Absent Absent
15	Rt. M5	17	1.0	Rt. inguinal ln	Fibroadenoma		Absent
16	Rt. M5 Lt. M5	111 24	1.0	Lt. inguinal ln Rt. inguinal ln	Carcinosarcoma Carcinosarcoma	III III	Present Absent
17	Lt. M4 Rt. M4	12 12	1.0	Lt. inguinal ln Rt. inguinal ln	Complex adenoma Benign mixed tumor		Absent Absent
18	Lt. M3 Lt. M4	8 21	0.5	Lt. axillary ln Lt. inguinal ln	Benign mixed tumor Benign mixed tumor		Absent Absent
19	Rt. M5	8	0.5	Rt. inguinal ln	Benign mixed tumor		Absent
20	Lt. M5	47	0.5	Not detected	Spindle cell carcinoma	III	Present
21	Rt. M1	40	0.5	Not detected	Anaplastic carcinoma	III	Present
22	Rt. M4	5	0.5	Rt. inguinal ln	Complex carcinoma	I	Absent
23	Lt. M4	7	0.5	Rt. inguinal ln	Complex carcinoma	I	Absent
24	Lt. M3 Rt. M3 Rt. M4	9 7 16	0.5	Lt. axillary ln Rt. inguinal ln Rt. inguinal ln	Complex adenoma Complex adenoma Benign mixed tumor		Absent Absent

Table 2. Tumor characteristics of canine mammary tumor patients undergoing indocyanine green near-infrared fluorescence-guided Sentinel lymph node mapping and lymphadenectomy. M, mammary gland; ln, lymph node; Lt, left; Rt, right

The lymphatic drainage and SLN of CMT were identified under ICG-NIRF (Fig. 1) and the detection rate of SLNs in CMT was 94.4% (34/36).

Both false-negative lymphatic drainages and LNs were identified in two tumors (5.6%, 2/36) at an ICG concentration of 0.5 mg/mL; however, LN biopsies were conducted based on anatomical landmarks. Additionally, a false-negative LN was detected at a dose of 2.5 mg/mL (2.8%, 1/36); but the fluorescence of lymphatic drainage was adequate to guide SLN biopsies (Fig. 2).

An ICG concentration of 2.5 mg/mL yielded the highest lymphatic duct fluorescence (mean, 4.8 ± 1.2; 95% CI, 3.7–5.9), but no significant difference was detected between 2.5 and 1.0 mg/mL ($p = 0.13$) concentrations. Both 2.5 mg/mL and 1.0 mg/mL concentrations demonstrated significantly greater lymphatic duct fluorescence compared to the 0.5 mg/mL concentration ($p < 0.001$ and $p = 0.003$, respectively). An ICG concentration of 1.0 mg/mL resulted in the highest LN fluorescence (mean, 10.9 ± 4.8; 95% CI, 6.9–14.9), which was significantly higher compared with that of the 2.5 mg/mL ($p = 0.030$) concentration. In terms of operation time, 1.0 mg/mL of ICG showed the shortest duration (mean, 4.9 ± 2.2; 95% CI, 3.5–6.3), which was statistically shorter compared with that for the 2.5 mg/mL concentration ($p = 0.002$).

Complications

No complications related to peritumoral ICG injections or intraoperative SLN biopsies were observed. Short-term (1 day, 3 days, 1 week, and 2 weeks) and long-term (6 weeks, and 3 months) complications of SLN biopsy were not observed.

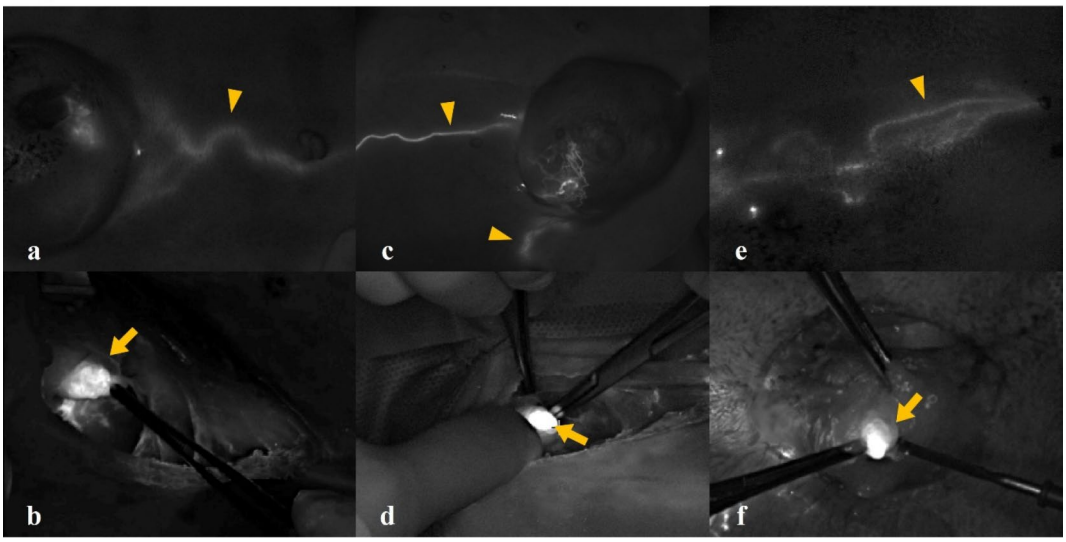

Fig. 1. Indocyanine green (ICG) near-infrared fluorescent images of lymphatic drainage (arrowhead) and sentinel lymph node (arrow) in canine mammary tumor. Three different concentrations of ICG were used for sentinel lymph node mapping of canine mammary tumors: (**a**, **b**) 2.5 mg/mL, (**c**, **d**) 1.0 mg/mL, and (**e**, **f**) 0.5 mg/mL.

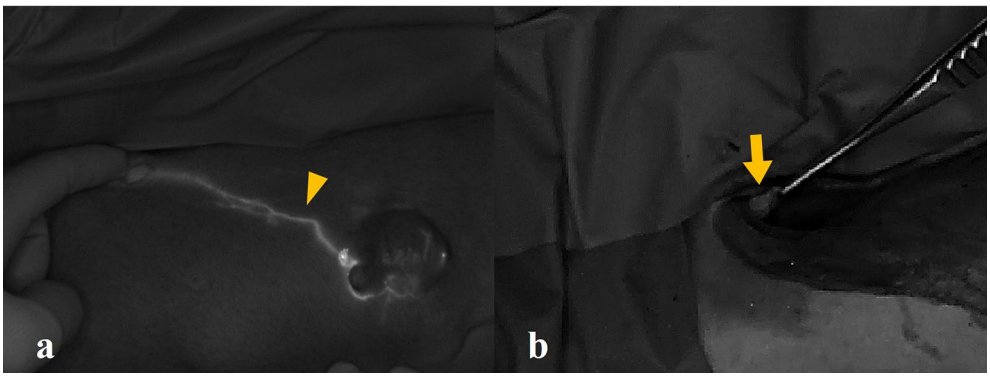

Fig. 2. (**a**) True-positive lymphatic drainage (arrowhead) and (**b**) false-negative sentinel lymph node (arrow) of the canine mammary tumor. The lymph node did not exhibit fluorescence, but the lymphatic drainage was sufficiently clear to guide the sentinel lymph node biopsy. This effect was observed in case no. 5, which has used an indocyanine green concentration of 2.5 mg/mL.

Discussion

In this study, the detection rate of SLNs in CMT using ICG-NIRF was 94.4%. Various techniques have been employed to identify LNs in canine tumors, including ICTL, patent blue dye, lymphoscintigraphy, and contrast-enhanced ultrasound[9–12]. While these methods have demonstrated high sensitivity (92–95%) for SLN detection, they have limitations such as the need for specialized technical expertise and equipment, patients' exposure to ionizing radiation, and the inability to detect SLNs in real-time[9,11,12]. ICG-NIRF is an emerging technique that has been successfully utilized for guided surgical tumor resection[17–22], cholangiography[23], tissue perfusion evaluation[24], and SLN mapping[12,14–16]. ICG-NIRF is noted for its SLN detection rate, which is comparable with or exceeds that of other modalities in canine tumors, with the added advantages of safety and real-time SLN mapping during surgery[14]. Additionally, using ICG-NIRF alone or in combination with other methods has shown similarly high detection rates with no significant differences in human breast cancer[25,26]. This study further confirmed that ICG-NIRF has a SLN detection rate comparable with or higher than that of established lymphography methods for CMT, validating its effectiveness for SLN mapping.

SLN mapping plays a crucial role in tumor staging and prognosis assessment[4]. While multiple SLNs were not observed in our study, previous research has reported cases of multiple SLNs identified using ICG-NIRF imaging in canine mast cell tumors, oral tumors, and insulinomas[14–16]. The presence of multiple SLNs impacts surgical decision-making, especially when tumor-induced atypical lymphatic drainage leads to unexpected SLNs outside

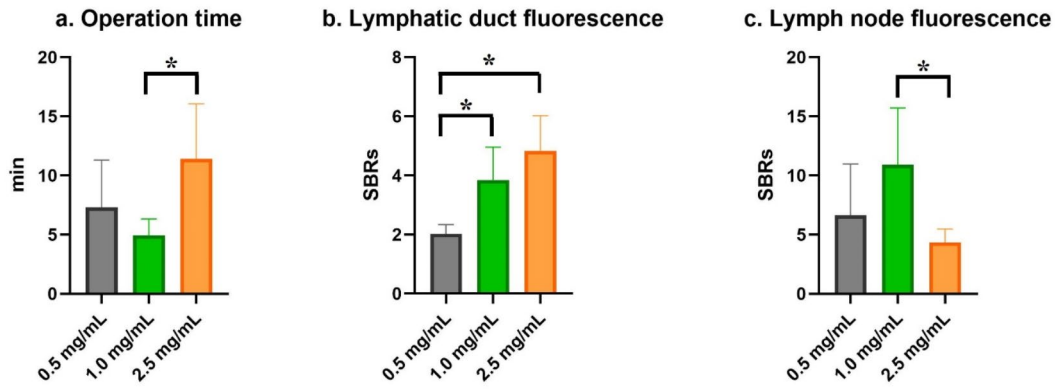

Fig. 3. A graph presenting the comparative analysis of operation time, lymphatic duct signal-to-background ratio (SBR), and lymph node SBR in canine mammary tumors using various concentrations of indocyanine green (ICG) (0.5, 1.0, and 2.5 mg/mL). The data were analyzed using ANOVA and post-hoc Tukey tests. (**a**) The operation time for the 0.5 mg/mL ICG concentration group was significantly shorter compared to the 2.5 mg/mL concentration group ($p = 0.002$). (**b**) The lymphatic duct SBR was significantly greater in both the 2.5 mg/mL and 1.0 mg/mL concentration groups compared to the 0.5 mg/mL group ($p < 0.001$ and $p = 0.003$, respectively). (**c**) The 1.0 mg/mL ICG concentration resulted in the highest lymph node SBR (mean, 10.9 ± 4.8; 95% confidence interval, 6.9–14.9), which was significantly higher than that of the 2.5 mg/mL concentration ($p = 0.030$).

	Dose		
	0.5 mg/mL(n=10)	**1.0 mg/mL(n=18)**	**2.5 mg/mL(n=10)**
Operation time in minutes (Mean ± SD)	7.3 ± 3.8 (95% CI, 3.3–11.3)	4.9 ± 2.2[a] (95% CI, 3.5–6.3)	11.4 ± 4.4[b] (95% CI, 6.8–16.1)
Lymphatic duct SBR (Mean ± SD)	2.0 ± 0.3[a] (95% CI, 1.7–2.3)	3.9 ± 1.1[b] (95% CI, 3.1–4.6)	4.8 ± 1.2[b] (95% CI, 3.7–5.9)
Lymph node SBR (Mean ± SD)	6.6 ± 4.4 (95% CI, 2.1–11.2)	10.9 ± 4.8[a] (95% CI, 6.9–14.9)	4.3 ± 1.1[b] (95% CI, 2.9–5.7)

Table 3. A comparative data of the operation time, lymphatic duct signal-to-background ratio (SBR), and lymph node SBR on canine mammary tumors with varying concentrations of indocyanine green (ICG). The study included three distinct concentration groups: 0.5 mg/ml ($n = 10$), 1.0 mg/ml ($n = 18$), and 2.5 mg/ml ($n = 10$). The results are presented as mean values and standard deviations, accompanied by their respective 95% confidence intervals for each ICG concentration. Statistically significant differences ($p < 0.05$, one-way ANOVA with Tukey's post hoc test) are indicated by different superscripts within a row. SBR, signal-to-background ratio; CI, confidence interval. Different superscripts within a row indicate statistically significant differences ($p < 0.05$)

traditional pathways[6,27]. From a post-surgical perspective, multiple SLNs may indicate a more advanced disease stage, influencing treatment strategies such as adjuvant therapy or additional surgical intervention. Although our study did not detect multiple SLNs, future studies with a larger cohort may further elucidate the role of real-time SLN mapping in staging and prognosis evaluation.

Metastatic infiltration was detected in four LNs (11.1%, 4/36). Previous research has shown that distant metastasis in malignant CMT can occur in regional LNs, lungs, liver, spleen, kidneys, and bones, with LN metastasis rates ranging from 11 to 44%[28,29]. The presence of metastatic LNs is associated with a poor prognosis. Earlier studies reported that canine patients with positive LNs have a shorter disease-free interval, with 80% experiencing tumor recurrence within 6 months[30]. Additionally, another study found a reduced 2-year survival rate in canine patients with malignant mammary tumors and LN metastasis[31]. In this study, a follow-up of at least 3 months post-surgery revealed no recurrence, metastasis, or mortality in canine patients without LN metastasis. In contrast, one canine patient with lymph node metastasis died 3 months post-surgery, while another canine patient was diagnosed with lung metastasis 1 month post-surgery.

The lymphatic drainage patterns in CMT using ICG-NIRF were investigated. Typically, the cranial mammary glands drain into the axillary or accessory axillary LNs, while the caudal mammary glands drain into the inguinal LNs[6]. However, regional lymph nodes do not necessarily serve as sentinel lymph nodes[6,27]. Malignant mammary tumors can metastasize to the sternal or medial iliac LNs and may involve both ipsilateral and contralateral

nodes[27]. This study observed a contralateral lymphatic drainage pattern in 11.1% (4/36) of the cases, indicating that biopsies could have been misdirected without ICG-NIRF. Moreover, tumors in the third mammary gland demonstrate variable drainage patterns, either cranial or caudal, underscoring the importance of lymphatic channel visualization for accurate SLN identification. Specifically, tumors in the third mammary gland exhibited cranial drainage in 5 cases and caudal drainage in 4 cases. Thus, precise SLN biopsy requires identification of the efferent lymphatic drainage of the tumor for effective mapping. The study successfully identified efferent lymphatic channels in 94.7% (36/38) of tumors, facilitating SLN biopsies.

We evaluated three different ICG doses (0.5, 1.0, and 2.5 mg/mL) to determine the optimal visualization of the lymphatic channels and SLNs. Previous research in both humans and dogs has used various ICG concentrations for SLN mapping, ranging from 0.25 to 2.5 mg/mL in cutaneous tumors[32]. Previous studies have proposed that 0.62 mg of ICG represents the optimal dosage for SLN mapping in human breast cancer[33–35]. However, a standardized protocol for SLN mapping with ICG-NIRF has not yet been established and there is limited evidence to support the use of various doses. This study compared the signal-to-background ratios (SBRs) to identify the optimal ICG dose for visualizing lymphatic drainage and LNs. Although 2.5 mg/mL of ICG provided the best lymphatic visualization, 1.0 mg/mL of ICG showed better LN visualization and false-negative LN results were observed in 2.5 mg/mL of ICG. At 1 mg/mL ICG, higher lymphatic visualization was noted compared with at 0.5 mg/mL ICG ($p = 0.003$), with no false-negative LNs, resulting in a 100% detection rate. Moreover, the shortest operation time was observed with 1 mg/mL ICG, indicating that the optimal dose improved visualization and reduced the operation time.

This study identified false-negative results for lymphatic drainage and LNs. False negatives in ICG-NIRF are associated with tumor-infiltrating lymphatic channels, prior surgery, and lymphedema[36–38]. In this study, tumors that showed no fluorescence in either the lymphatic drainage or LNs were histopathologically confirmed to have tumor-infiltrating lymphatic channels. Tumor infiltration into lymphatic channels can impair or block lymphatic drainage, thereby diminishing ICG detection sensitivity. Additionally, at an ICG concentration of 2.5 mg/mL, the lymphatic channels exhibited fluorescence, whereas the lymph nodes did not. This observation may be attributed to the quenching effect of ICG. The ICG quenching effect, where the fluorescence intensity of ICG diminishes under specific conditions, usually occurs due to high concentration aggregation, reducing the sensitivity of LN detection[13]. To minimize false-negative results, an optimal ICG dose for SLN mapping is necessary, and a biopsy should be considered even if fluorescence is not observed intraoperatively.

Complications following lymphadenectomy include infection, seroma, hematoma, dehiscence, and lymphedema, primarily resulting from damage to the lymphatic duct or surrounding structures during biopsy[39]. Unlike conventional lymphadenectomy, ICG-NIRF-guided lymphadenectomy reduces damage to the lymphatic vessels and adjacent tissues by allowing real-time visualization of lymphatic drainage during biopsy. Additionally, the identification of SLNs reduces unnecessary biopsies, thereby minimizing potential intraoperative and postoperative complications. This study observed no lymphatic duct damage during surgery and reported no lymphadenectomy-related complications during the follow-up period of 3 months. Consequently, ICG-NIRF enables precise and safe SLN biopsy.

This study had some limitations. First, its small sample size is a limitation, and future studies need to be conducted with larger samples to validate the clinical utility of ICG-NIRF for SLN mapping. Additionally, the large standard deviations in operation time and LN SBRs may reflect interindividual variability among the subjects. Increasing the sample size in future studies may help reduce this variability and provide more precise and generalizable estimates. Although the sample sizes are small, this study suggests that specific ICG concentrations may be useful in SLN procedures. These findings provide valuable preliminary data that can inform future clinical applications. For false-negative lymphatic drainage and LNs, we hypothesized that fluorescence would not occur because of tumor infiltration. However, the possibility of a low ICG concentration causing this effect cannot be excluded and warrants further investigation with a larger sample size. Moreover, ICG-NIRF has a reduced sensitivity for deep LNs. Malignant CMT may drain into the sternal or medial iliac LNs located within the abdominal or thoracic cavity, making detection challenging and possibly requiring additional biopsy incisions. In this study, the SLNs identified by ICG-NIRF were located in the subcutaneous tissue, making biopsy feasible. However, if the SLN is located within the thoracic or abdominal cavity, an additional incision may be necessary. Therefore, further research is needed to explore the application of modalities, such as ICTL and lymphoscintigraphy, before surgery. A control group was not included due to ethical considerations regarding the use of untreated animals. However, future studies should incorporate a control group to better evaluate the efficacy of ICG-NIRF.

In conclusion, this study successfully utilized ICG-NIRF for the SLN mapping of CMT. Transcutaneous injection of ICG allows for intraoperative visualization of efferent lymphatic channels and LNs, facilitating SLN biopsy with a high detection rate. Additionally, we determined the optimal ICG dose for SLN mapping by comparing the SBRs of the lymphatic drainage and LNs at different ICG dosages. This optimal dose has potential applications in SLN mapping of other human and canine malignancies.

Methods

Ethical approval

All dogs were patients at the Department of Veterinary Surgery, Chungbuk National University Veterinary Teaching Hospital. Written informed consent was obtained from the respective owners, and all the procedures were approved by the Chungbuk National University Institutional Animal Care and Use Committee (CBNUA-24–0036-03). This study was conducted in accordance with relevant guidelines and in compliance with the ARRIVE 2.0 guidelines.

Study population

Client-owned dogs with CMTs were prospectively recruited between September 2023 and April 2024. The inclusion criterion was a cytological diagnosis of malignant mammary tumors. The exclusion criteria included a previous history of mammary surgery or locoregional lymphadenectomy.

The following clinical data were collected for all the canine patients: breed, sex, age, body weight, body condition score (ranging from 1 to 9), tumor location, and tumor size (measured as the maximum diameter in mm). Presurgical staging was performed 2 weeks before surgery, and included FNA of the tumors and enlarged LNs, thoracic and abdominal radiography, and abdominal ultrasonography. If distant metastases were detected, surgery was not performed.

Intraoperative NIRF and SLN biopsy

SLN biopsy was performed for at least one lymphadenectomy of a tumor, either with intraoperative NIRF or based on the anatomical location. All surgeries were performed by an expert surgeon. Anesthesia was induced with intravenous propofol (4–6 mg/kg; Freefol-MCT, Daewon Pharm. Co., Ltd., Seoul, South Korea). All procedures were conducted under general anesthesia with 2.0% isoflurane (Terrell, Piramal Critical Care, Bethlehem, PA, USA), 100% oxygen ventilation, and intravenous infusion of Hartmann's solution (2–4 mL/kg/h). A 2.5 mg/mL solution of ICG (Cellbion Green, Cellbion Co., Ltd., Seoul, South Korea) was prepared by mixing 25 mg of ICG with 10 mL of sterile water. This solution was then diluted with 0.9% NaCl, resulting in ICG mixtures with concentrations of 2.5, 1.0, and 0.5 mg/mL. Subsequently, 0.5 mL of these mixtures were injected peritumorally into four quadrants (0.125 mL/quadrant) for each tumor. In cases where a dog had multiple CMTs, ICG was injected into the largest tumor within the same anatomical lymphatic chain to ensure accurate sentinel lymph node mapping while avoiding overlap of the fluorescent signal. ICG concentration groups were randomly assigned using a computer-generated schedule to ensure an unbiased distribution. A 26G needle was used to minimize leakage. After injection, a gauze was applied to prevent leakage and contamination of the NIRF field by ICG. The used needle was replaced before injecting at a different site. Subsequently, ICG fluorescence imaging was performed using a near-infrared camera system (Metaple Bio Inc., Seoul, South Korea), and images were recorded using fluorescence intensity analysis software (MGViewer V1.1.1, MetapleBio Inc., Seoul, South Korea). The NIRF camera was positioned 10–15 cm above the skin surface. A gentle massage was applied after injection to aid visualization, and lymphatic drainage was visible within 5 min. Lymphatic drainage was observed using NIRF, and the fluorescence intensity was recorded as the mean SBRs. Due to interindividual variability in the time required for lymphatic channel visualization, SBR was not quantified based on a fixed injection time. Instead, SBR was measured 1 min after the lymphatic channels became visible, ensuring a standardized comparison across subjects. The areas suspected to be SLNs were marked using surgical markers. If LNs were deep and not visible, the point at which the fluorescence signal ended was marked with a surgical marker, and an incision was made at that point. The LNs were confirmed by NIRF after incision, and careful blunt dissection was performed to expose the LNs without damaging the lymphatic tract. The fluorescence intensity in the LNs was recorded as the mean SBRs. The LNs were delineated using NIRF for margin setting and then subjected to lymphadenectomy. If the SLN did not fluoresce, but the regional lymphatics did, indicating the location of the SLN, the LN was considered SLN and was surgically biopsied. The operative time for lymphadenectomy was measured from incision to LN dissection.

Surgical procedure and postoperative outcomes

CMT surgery was performed after lymphadenectomy, and ovariohysterectomy was performed before mastectomy when necessary. The incision line was determined based on the tumor size and lymphatic drainage of the primary tumor. Complications were categorized as intraoperative or postoperative. Postoperative complications were assessed 1 day, 3 days, 1 week, 2 weeks, 6 weeks, and 3 months after surgery.

Histopathological examination

The resected LNs and primary tumors were immediately fixed in 10% formaldehyde and sent to IDEXX laboratories (IDEXX Laboratories, Inc., USA) for histopathological analysis the following day. Routine hematoxylin and eosin staining was performed for the histological evaluation of the LNs and tumors. Descriptive comparisons were made regarding tumor type, histologic tumor grade, and histopathologic LN metastasis.

Data analysis

The LN detection rate was determined by comparing the identified and biopsied LNs under NIRF guidance to the planned SLN biopsies. LN detection was validated by histopathological examination. The mean SBRs of lymphatic drainage and LNs were calculated by comparing their signal intensities with those of adjacent non-ICG-contaminated tissues. The operation time for SLN dissection was measured from the initial incision to the completion of lymphadenectomy. The nodal metastasis rate was computed by comparing the dissected LNs that were histologically confirmed as tumor-positive to the total number of dissected LNs.

Statistical analyses were performed using the Statistical Package for the Social Sciences (IBM SPSS Statistics V28.0, IBM Corp., Armonk, NY, USA). Descriptive analysis summarized the data. Continuous variables (age, body weight, tumor size, SBRs of lymphatic drainage and lymph nodes, and operation time) were presented as mean, median and 95% CI, while ordinal scale data (BCS) were expressed as median and range. Categorical variables (breed, sex, tumor location, draining lymph nodes, tumor type, tumor grade, and lymph node metastasis) were reported as absolute and relative frequencies. One-way Analysis of Variance was used to analyze the differences in age, body weight, BCS, tumor size, SBRs of lymphatic drainage and LNs, and operation time among the different ICG concentration groups (0.5, 1.0, 2.5 mg/mL). Post-hoc analysis using Tukey's multiple

comparison tests was conducted to compare the different ICG concentration groups. Statistical significance was set at a p-value of less than 0.05.

Data availability

All data generated or analyzed during this study are included in this published article. The datasets generated during and/or analyzed during the current study are available from the corresponding author on reasonable request.

Received: 5 August 2024; Accepted: 26 February 2025
Published online: 10 March 2025

References

1. Vascellari, M. et al. Incidence of mammary tumors in the canine population living in the Veneto region (Northeastern Italy): risk factors and similarities to human breast cancer. *Prev. Vet. Med.* **126**, 183–189 (2016).
2. Zheng, H. H. et al. Epidemiological investigation of canine mammary tumors in Mainland China between 2017 and 2021. *Front. Vet. Sci.* **9**, 843390 (2022).
3. Pastor, N. et al. Epidemiological study of canine mammary tumors: age, breed, size and malignancy. *Austral J. Vet. Sci.* **50** (3), 143–147 (2018).
4. Withrow, S. J., Page, R. & Vail, D. M. Withrow and MacEwen's small animal clinical oncology (ed. Karin, U.) 607–608Elsevier Health Sciences, (2012).
5. Owen, L. *TNM Classification of Tumors in Domestic Animals* 1st edn (World Health Organization, 1980).
6. Pereira, C. T., Rahal, S. C., de Carvalho Balieiro, J. C. & Ribeiro, A. A. Lymphatic drainage on healthy and neoplasic mammary glands in female dogs: can it really be altered? *Anat. Histol. Embryol.* **32**, 282–290 (2003).
7. Burak, W. E. et al. Sentinel lymph node biopsy results in less postoperative morbidity compared with axillary lymph node dissection for breast cancer. *Am. J. Surg.* **183** (1), 23–27 (2002).
8. Williams, L. E. & Packer, R. A. Association between lymph node size and metastasis in dogs with oral malignant melanoma: 100 cases (1987–2001). *J. Am. Vet. Med. Assoc.* **222**, 1234–1236 (2003).
9. Soultani, C. et al. Assessment of Sentinel lymph node metastasis in canine mammary gland tumors using computed tomographic indirect lymphography. *Vet. Radiol. Ultrasound.* **58**, 186–196 (2017).
10. Souza, M. C. C. et al. Comparison of surgical resection of axillary lymph nodes in dogs with mammary gland tumors with or without Sentinel lymph node visualization with patent blue dye. *Front. Vet. Sci.* **10**, 1149315 (2023).
11. Manfredi, M. et al. Preoperative planar lymphoscintigraphy allows for Sentinel lymph node detection in 51 dogs improving staging accuracy: feasibility and pitfalls. *Vet. Radiol. Ultrasound.* **62**, 602–609 (2021).
12. Favril, S. et al. Sentinel lymph node mapping by near-infrared fluorescence imaging and contrast-enhanced ultrasound in healthy dogs. *Vet. Comp. Oncol.* **17** (1), 89–98 (2019).
13. Reinhart, M. B., Huntington, C. R., Blair, L. J., Heniford, B. T. & Augenstein, V. A. Indocyanine green: historical context, current applications, and future considerations. *Surg. Innov.* **23**, 166–175 (2016).
14. Beer, P., Rohrer-Bley, C. & Nolff, M. C. Near-infrared fluorescent image-guided lymph node dissection compared with locoregional lymphadenectomies in dogs with mast cell tumours. *J. Small Anim. Pract.* **63**, 670–678 (2022).
15. Wan, J., Oblak, M. L., Ram, A., Singh, A. & Nykamp, S. Determining agreement between preoperative computed tomography lymphography and indocyanine green near infrared fluorescence intraoperative imaging for Sentinel lymph node mapping in dogs with oral tumours. *Vet. Comp. Oncol.* **19** (2), 295–303 (2021).
16. Nolff, M. C., Dennler, R. & Dennler, M. Use of indocyanine green near-infrared lymphography to detect Sentinel lymph nodes in a dog with a malignant insulinoma: a case report. *Front. Vet. Sci.* **10**, 1178454 (2023).
17. Yu, S. Y. & Lee, S. Imaging guided adrenalectomy with indocyanine green fluorescence in a dog with a pheochromocytoma. *J. Vet. Sci.* **25**, e53 (2004).
18. Holt, D. et al. Intraoperative near-infrared fluorescence imaging and spectroscopy identifies residual tumor cells in wounds. *J. Biomed. Opt.* **20** (7), 076002–076002 (2015).
19. Madajewski, B. et al. Intraoperative near-infrared imaging of surgical wounds after tumor resections can detect residual disease. *Clin. Cancer Res.* **18** (20), 5741–5751 (2012).
20. Iida, G. et al. Intraoperative identification of canine hepatocellular carcinoma with indocyanine green fluorescent imaging. *J. Small Anim. Pract.* **54** (11), 594–600 (2013).
21. Holt, D. et al. Intraoperative near-infrared imaging can distinguish cancer from normal tissue but not inflammation. *PLoS One.* **9** (7), e103342 (2014).
22. Favril, S. et al. Fluorescence-guided surgery using indocyanine green in dogs with superficial solid tumours. *Vet. Rec.* **187** (7), 273–273 (2020).
23. Kim, S. H. & Lee, S. Determining the patency of biliary tracts in dogs with gallbladder mucocele using near-infrared cholangiography with indocyanine green. *PLoS One.* **19**, e0300395 (2024).
24. Eiger, S. N. et al. Use of near-infrared fluorescence angiography with indocyanine green to evaluate direct cutaneous arteries used for canine axial pattern flaps. *Vet. Surg.* **53**, 1073–1082 (2024).
25. Ji, Y. et al. Clinical utility of the additional use of blue dye for indocyanine green for Sentinel node biopsy in breast cancer. *J. Surg. Res.* **215**, 88–92 (2017).
26. Ngô, C. et al. Indocyanine green for Sentinel lymph node detection in early breast cancer: prospective evaluation of detection rate and toxicity—The FLUOBREAST trial. *Breast J.* **26**, 2357–2363 (2020).
27. Patsikas, M. N. et al. The lymph drainage of the neoplastic mammary glands in the bitch: a lymphographic study. *Anat. Histol. Embryol.* **35**, 228 (2006).
28. Chang, S. C., Chang, C. C., Chang, T. J. & Wong, M. L. Prognostic factors associated with survival two years after surgery in dogs with malignant mammary tumors: 79 cases (1998–2002). *J. Am. Vet. Med. Assoc.* **227**, 1625 (2005).
29. Schafer, K. A. et al. A canine model of Familial mammary gland neoplasia. *Vet. Pathol.* **35**, 168 (1998).
30. Kurzman, I. D. & Gilbertson, S. R. Prognostic factors in canine mammary tumors. *Semin Vet. Med. Surg. (Small Anim).* **1**, 25 (1986).
31. Karayannopoulou, M., Kaldrymidou, E., Constantinidis, T. C. & Dessiris, A. Histological grading and prognosis in dogs with mammary carcinomas: application of a human grading method. *J. Comp. Pathol.* **133**, 246 (2005).
32. Beer, P., Chiti, L. E. & Nolff, M. C. The role of Sentinel node mapping and lymphadenectomies in veterinary surgical oncology. *Lymphatics* **1**, 2–18 (2023).
33. van der Vorst, J. R. et al. Randomized comparison of Near-infrared fluorescence imaging using indocyanine green and 99(m) technetium with or without patent blue for the Sentinel lymph node procedure in breast Cancer patients. *Ann. Surg. Oncol.* **19**, 4104–4111 (2012).

34. Mieog, J. S. et al. Toward optimization of imaging system and lymphatic tracer for near-infrared fluorescent Sentinel lymph node mapping in breast cancer. *Ann. Surg. Oncol.* **18**, 2483–2491 (2011).
35. Hutteman, M. et al. Randomized, double-blind comparison of indocyanine green with or without albumin premixing for near-infrared fluorescence imaging of Sentinel lymph nodes in breast cancer patients. *Breast Cancer Res. Treat.* **127**, 163–170 (2011).
36. Kwon, I. G., Son, T., Kim, H. I. & Hyung, W. J. Fluorescent lymphography-guided lymphadenectomy during robotic radical gastrectomy for gastric cancer. *JAMA Surg.* **154**, 150–158 (2019).
37. Goyal, A., Newcombe, R. G., Chhabra, A., Mansel, R. E. & ALMANAC Trialists Group. Factors affecting failed localisation and false-negative rates of Sentinel node biopsy in breast cancer – results of the ALMANAC validation phase. *Breast Cancer Res. Treat.* **99**, 203–208 (2006).
38. Tonouchi, H. et al. Laparoscopic lymphatic mapping and Sentinel node biopsies for early-stage gastric cancer: the cause of false negativity. *World J. Surg.* **29**, 418–421 (2005).
39. Chiti, L. E. et al. Surgical complications following Sentinel lymph node biopsy guided by γ-probe and methylene blue in 113 tumour-bearing dogs. *Vet. Comp. Oncol.* **21**, 62–72 (2023).

Acknowledgements
The authors would like to thank the owners of the dogs for consenting to publish this report. The authors would like to thank Yujin Kim for assistance in formatting the tables and figures.

Author contributions
Conceptualization: S.K., S.L.; Data curation: S.K.; Formal analysis: S.K.; Funding acquisition: S.K., S.L.; Resources: S.K.; Software: S.K.; Supervision: S.L.; Validation: S.L.; Visualization: S.K., S.L.; Writing - original draft: S.K., S.L.; Writing - review & editing: S.K., S.L.

Funding
This work was supported by the National Research Foundation of Korea (NRF) grant funded by the Korea government (MSIT) (RS-2024-00394639) and also supported by the Basic Research Lab Program (2022R1A4A1025557) through the National Research Foundation (NRF) of Korea, funded by the Ministry of Science and ICT.

Declarations

Competing interests
The authors declare no competing interests.

Additional information
Correspondence and requests for materials should be addressed to S.L.

Reprints and permissions information is available at www.nature.com/reprints.

Publisher's note Springer Nature remains neutral with regard to jurisdictional claims in published maps and institutional affiliations.